Check for updates

doi.org/10.1002/cbdv.202100646

FULL PAPER

CHEMISTRY & BIODIVERSITY

An Allosteric Inhibitory Potential of Triterpenes from *Combretum racemosum* on the Structural and Functional Dynamics of *Plasmodium falciparum* Lactate Dehydrogenase Binding Landscape

Wande M. Oluyemi,[a] Babatunde B. Samuel,[a] Adeniyi T. Adewumi,*[b] Yemi A. Adekunle,[a, c] Mahmoud E. S. Soliman,[b] and Liselotte Krenn*[d]

[a] Laboratory for Natural Products and Biodiscovery Research, Pharmaceutical Chemistry Department, Faculty of Pharmacy, University of Ibadan, Nigeria

[b] Molecular Bio-computation and Drug Design Laboratory, School of Health Sciences, University of KwaZulu-Natal, Westville Campus, Durban 4001, South Africa, e-mail: jesutomisin0707@gmail.com

[c] Department of Pharmaceutical Chemistry, Dora Akunyili College of Pharmacy, Igbinedion University, Okada, Benin City, Nigeria

[d] Department of Pharmacognosy, University of Vienna, Althanstrasse 14, A-1090 Vienna, Austria, e-mail: liselotte.krenn@univie.ac.at

© 2022 The Authors. Chemistry & Biodiversity published by Wiley-VHCA AG. This is an open access article under the terms of the Creative Commons Attribution Non-Commercial NoDerivs License, which permits use and distribution in any medium, provided the original work is properly cited, the use is non-commercial and no modifications or adaptations are made.

Multidrug resistance is a significant drawback in malaria treatment, and mutations in the active sites of the many critical antimalarial drug targets have remained challenging. Therefore, this has necessitated the global search for new drugs with new mechanisms of action. *Plasmodium falciparum* lactate dehydrogenase (*pf*LHD), a glycolytic enzyme, has emerged as a potential target for developing new drugs due to the parasite reliance on glycolysis for energy. Strong substrate-binding is required in *pf*LDH enzymatic catalysis; however, there is a lack of information on small molecules' inhibitory mechanism bound to the substrate-binding pocket. Therefore, this study investigated a potential allosteric inhibition of *pf*LDH by targeting the substrate-binding site. The structural and functional behaviour of madecassic acid (MA), the most promising among the six triterpenes bound to *pf*LDH, were unravelled using molecular dynamic simulations at 300 ns to gain insights into its mechanism of binding and inhibition and chloroquine as a standard drug. The docking studies identified that the substrate site has the preferred position for the compounds even in the absence of a co-factor. The bound ligands showed comparably higher binding affinity at the substrate site than at the co-factor site. Mechanistically, a characteristic loop implicated in the enzyme catalytic activity was identified at the substrate site. This loop accommodates key interacting residues (LYS174, MET175, LEU177 and LYS179) pivotal in the MA binding and inhibitory action. The MA-bound *pf*LHD average RMSD (1.60 Å) relative to chloroquine-bound *pf*LHD RMSD (2.00 Å) showed higher stability for the substrate pocket, explaining the higher binding affinity (−33.40 kcal/mol) observed in the energy calculations, indicating that MA exhibited profound inhibitory activity. The significant *pf*LDH loop conformational changes and the allostery substrate-binding landscape suggested inhibiting the enzyme function, which provides an avenue for designing antimalarial compounds in the future studies of *pf*LDH protein as a target.

Keywords: Madecassic acid, *Plasmodium falciparum* lactate dehydrogenase (*pf*LDH), antimalarial, molecular dynamic simulations, multidrug resistance.

1. Introduction

Malaria is a vector-borne infectious disease that is common in tropical and subtropical regions. *Plasmodium falciparum* causes the most severe, virulent and frequent disease through the bite of female anopheles mosquito carrying blood infected with plasmodia parasites;[1,2] and it is also responsible for most fatal cases.[3] Based on the World Malaria Report of 2018,

malaria cases were estimated to be 228 million and 405,000 deaths globally.[4]

Many clinically antimalarial drugs, including quinine, chloroquine, mefloquine, amodiaquine, artemisinins, target the erythrocytic or blood stage of the plasmodium lifecycle. A few other malarial drugs, such as primaquine, inhibit the extra-erythrocytic or hepatic drugs.[1,5] Although some of these drugs have been used for many years, multidrug resistance has necessitated the global search for new drugs with new mechanisms of action. Resistance is understood to be a result of mutations in the active sites of the target, not allowing the target to bind as effectively to the drug.[6,7] Mutation of *Plasmodium falciparum* multidrug resistance-1 (*pf*mdr-1) and *Plasmodium falciparum* chloroquine resistance transporter (*pf*crt) are implicated in chloroquine resistance and atavaquone resistance due to the mutation of Cytochrome *b* gene. Antifolates resistance occurred due to point mutations in the dihydrofolate reductase (dhfr), dihydropteroate synthase (dhps) proteins, and *P. falciparum* kelch-like proteins. Moreover, mutations have been reported against artemisinin and its derivatives drug resistance.[8] *Pf*mdr-1 dominates the digestive vacuole membrane and is responsible for multidrug resistance by directing xenobiotics away from the cytosol. Both chloroquine-resistant and -sensitive strains of *P. falciparum* show *pf*mdr-1 point mutations. N86Y, N1042D, S1034C and D1246Y single nucleotide polymorphisms (SNPs) were identified in *pf*mdr-1 gene, in which tyrosine, aspartic acid, cysteine and tyrosine replaced asparagine at codons 86 and 1042, serine at codon 1034 and aspartic acid at codon 1246 of *pf*mdr-1 protein, respectively. These substitutions have altered the physicochemical properties of P-glycoprotein (P-gp) as all the substituted amino acids are more polar compared to their substituents.[9] Hence, new antimalarial agents may be developed to overcome drug resistance by identifying the main targets of the drugs and thoroughly understanding the mechanism of action concerning these targets.

Malarial parasites have a high level of glucose consumption during their erythrocytic stage.[10,11] *Plasmodium* is ultimately dependent on glucose metabolism for ATP production. Several glycolytic enzymes are upregulated in the host's red blood cells depending on parasitemia levels.[12] *Plasmodium falciparum* lactate dehydrogenase (*pf*LDH) is a glycolytic enzyme that is important for the anaerobic lifestyle of the parasite.[13] *Pf*LDH is structurally, functionally and biochemically distinct from that of the human host cell.[14] The crystal structure of *pf*LDH has a significant shift in the position of the NADH co-factor from that of the human enzyme. Consequently, this is responsible for its different biochemical features. The alignment of the crystal structures of *Plasmodium falciparum* LDH and human LDH–A by Alam *et al.*[15] revealed two regions of structural differences between them at the substrate specificity loop and the antigenic loop. It is, therefore, a selective target for drug discovery intervention. The normal glycolytic function of p*f*LDH is to catalyse the interconversion of pyruvate to lactate in the final step of glycolysis.[15] Strong substrate-binding and product release are required in *pf*LDH enzymatic catalysis. Several studies have shown the substrate-binding pocket in *pf*LDH as an important druggable binding site with the possibility of allosteric inhibition of the catalytic activity.[7,16,17] The binding of the substrate to LDH necessarily happens before the formation of the LDH/NADH binary complex, which regulates the oligomeric protein folding, leading to dynamic change in enzyme activity.[18,19] The substrate-binding pocket, which accommodates HIS195 crucial in enzyme catalysis, is bound approximately 10 Å deep into the LDH + NADH + Substrate ternary complex. Also, the active site contains a catalytically crucial residue ARG109 located on a surface group of amino acids (residues 98–110) called the mobile loop. The loop is lowered deep proximal to the substrate within the active site, as the bound substrate and NADH are brought close to each other in a proper geometry having the enzyme tightens around them to enable them to react together. Thus, the pyruvate and NADH are activated for enzymatic catalysis by these structural changes of the protein.[16] The rate-limiting step in the dynamic enzyme activity of LDH is the final closure of the mobile loop over the substrate-binding pocket and not the chemical hydride transfer step.[20] Substantial motions within the proteins complex are required for a successful protein-ligand binding, including desolvation and closure of the binding pocket and supply of crucial amino acid groups into the active site. In this process, the active site loop undergoes dynamic motions, in which the open form facilitates ligand binding and release, while the closed-form enables preparation, control and protection of the reacting species.[20]

Inhibitors' activity through the substrate-binding pathway can seize the LDH substrate binding sites and reduce the enzyme activity.[16,19] Our recent work reported the isolation of antimalarial triterpenoids from a leaf extract of *Combretum racemosum* P. Beauv., with proven activity against chloroquine-sensitive (D10) and chloroquine-resistant (W2) strains of *Plasmo-*

 © 2022 The Authors. Chemistry & Biodiversity Published by Wiley-VHCA AG

dium falciparum, and MA demonstrated the highest activity (IC_{50}; D10: 28 ± 12 μg/mL, IC_{50}; W2: 17 ± 4 μg/mL) compared to the others.[21] These include madecassic acid (MA), arjungenin (ARJ), 6β,23-dihydroxytormentic acid (DHT), combregenin (CBG), terminolic acid (TA) and 19α-hydroxyasiatic acid (HAA). The molecular interactions of these triterpenes with potential malarial targets have not yet been reported in the literature. This study investigates the dynamics and motions of *pf*LDH protein through an alternative substrate-binding site to establish the mechanism of inhibition and the inhibitory potential of these triterpenes using molecular docking and molecular dynamics (MD) simulation of MA-bound *pf*LDH.

2. Methodology

2.1. System Preparation

2.1.1. Retrieval and Preparation of Protein

For the preparation of the protein target, the three-dimensional structure of *pf*LDH bound with its co-crystallised inhibitor, chloroquine (PDB ID: 1CEQ, Resolution: 2.05 Å),[22] was retrieved from Protein Data Bank (PDB). The protein crystal structure was pre-treated before docking using UCSF Chimera 1.14 tool.[23] The non-standard residues, including ions, water and bound ligands, were removed. The structural minimisation of the proteins was carried out at 200 steepest descent steps, 0.02 steepest descent steps size (Ă), ten conjugate gradient steps, and 0.02 conjugate gradient steps size (Ă) 10 update intervals using the structure editing wizard. Solvents were removed, hydrogen bonds were added, charges were assigned using the Gasteiger force field, histidine was set for the protonation state.[23] Every available selenomethione (MSE) was changed to methionine (MET), bromo-UMP (5BU) to UMP (U), methylselenyl-dUMP (UMS) to UMP (U) and methylselenyl-dCMP (CSL) to CMP (C).[23]

2.1.2. Ligand Selection and Preparation

Ligands used in this study are chemical structures of arjungenin (ARJ), 19α-hydroxyasiatic acid (HAA), 6β,23-dihydroxytormentic acid (DTA), combregenin (CBG), madecassic acid (MA) and terminolic acid (TA), which are antiplasmodial compounds from *Combretum racemosum*. The structure data file (SDF) format of ARJ, MA, TA and chloroquine (CQ) as standard inhibitor were obtained from the PubChem database. HAA, DTA, CBG were drawn with MarvinSketch 20.20. PDB coordinates of all ligand molecules were optimised by the UCSF Chimera tool, and charges were computed and added to the ligands through ANTECHAMBER.[24] The chemical structures of the ligands used in this study are shown in *Figure 1*.

2.2. Molecular Docking

The prepared proteins and ligands were uploaded to the PyRx-Virtual Screening Tool workspace. A blind docking was initially carried out where the ligands were docked to the whole surface of the protein, followed by a site-specific docking to the co-factor and substrate binding pocket as identified in a previous study.[7] Using the Autodock Vina of PyRx software, the grid box was set for docking based on the dimensions of the protein structure; each ligand-receptor binding

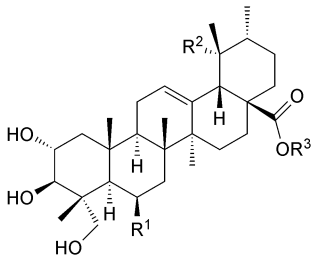

	R^1	R^2	R^3
HAA	H	OH	H
DTA	OH	OH	H
MA	OH	H	H

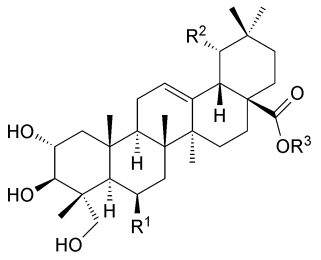

	R^1	R^2	R^3
ARJ	H	OH	H
CBG	OH	OH	H
TA	OH	H	H

Figure 1. Structures of antimalarial compounds from *Combretum racemosum*.

 © 2022 The Authors. Chemistry & Biodiversity Published by Wiley-VHCA AG

was set to have eight exhaustive conformations.[25] Post-docking analysis and visualisation were conducted by uploading the output files to the Chimera 1.14 workspace.[23] *Figure 2* shows the structure of *pf*LDH protein with docked ligands at both substrate and co-factor binding sites.

2.3. Molecular Dynamics (MD) Simulations

The UCSF Chimera was further used for the pre-MD preparations of the systems (ligand and receptor), as reported in a previous study.[26] The MD simulation studies were run for the *pf*LDH protein complexed with the most promising compound and the standard drug chloroquine using the graphic processor unit (GPU) version of the PMEMD.CUDA engine furnished with the AMBER package, FF18SB variant of the AMBER forcefield used to describe the protein.[27] The stability of the docked protein-ligand complexes was analysed by carrying out MD simulations studies. The GENERAL AMBER Forcefield (GAFF) and the restrained electrostatic potential (RESP) procedures were utilised by adding partial charges to the ligands was enhanced through ANTECHAMBER.[28] The neutralisation and solvation of the unbound *pf*LDH and ligand-bound systems were carried out using the LEAP module in AMBER 18 by adding charges; H^+, Na^+ and Cl^- counter ions. Furthermore, all-atoms explicit solvation was carried out in an orthorhombic TIP3P box of water molecules sized 10 Å. The procedure considered the initial minimisation of 2500 steps with an applied restrained potential of 500 kcal mol^{-1}. Complete minimisation (5000 steps) was additionally performed through a conjugate algorithm without utilising restraining conditions. Gradual heating of the systems was conducted beginning from 0 to 300 K for 50 ps, which was to enable the maintenance of a fixed volume and number of atoms considering a canonical ensemble (NVT). The shake algorithm was used to reduce the hydrogen bond constraint by applying one bar pressure used by the Barendsen-Barostat.[29,30] The total duration for running the MD simulations was 300 ns with a time scale of 2 fs using a Langevin thermostat, at 300 K, and 1 bar constant pressure. The coordinates of the Apo-*pf*LDH and bound-*pf*LDH complexes were saved every 1 ps, and the CJTRAJ and PTRAJ module in AMBER 18/GPU was used to analyse the trajectories. All analysed trajectories were studied for RMSD, RMSF, DSSP, DCCM, and radius of gyration using CPTRAJ and PTRAJ. The analyses of post-MD structures and visualisation[31] were done by employing the graphical user interface of UCSF Chimera and Discovery studio 2020 client to enable the study of the mechanism of binding of the ligand-bound systems,[32] and MicroCAl Origin 6.0 software for data analysis was used to plot the data.[27,33]

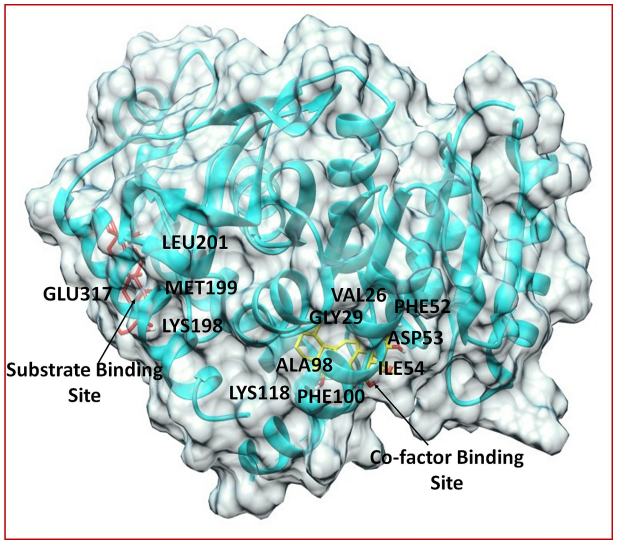

Figure 2. Structure of *pf*LDH showing the co-factor and substrate binding sites.

2.4. Post Molecular Dynamics (MD) Analysis

2.4.1. Binding Free Energy (BFE) Calculations

The investigation of the mechanism of biological processes is mainly carried out through molecular dynamics by employing the differences in free energy.[34] Molecular dynamics is a crucial computational method in studying the dynamics of proteins that comprehensively determine the binding mechanism of the receptor-ligand interacting systems. The molecular mechanics/generalised-born surface area (MM/GBSA) method calculated the protein system's binding free energy (BFE).[35] With the aid of the MM/GBSA technique, the BFE was utilised to estimate the binding affinities within the docked receptor-ligand systems to gain insights into their binding landscape.[30] The calculated energies utilised over 300 000 snapshots from the 300 ns trajectories. The MM/GBSA protocol requires complete removal of the used solvent and replacement by a dielectric continuum. The BFE (△G) calculated for madecassic acid- and chloroquine-bound *pf*LDH and the unbound systems was expressed as follows:

$$\Delta G_{bind} = \Delta G_{complex} - \Delta G_{receptor} - \Delta G_{ligand}$$

 © 2022 The Authors. Chemistry & Biodiversity Published by Wiley-VHCA AG

$$\Delta G_{bind} = E_{gas} + G_{sol} - T\Delta S$$

$$E_{gas} = E_{int} + E_{vdw} + E_{ele}$$

$$G_{sol} = G_{GB} + G_{SA}$$

$$G_{SA} = \gamma SASA$$

$\triangle G_{bind}$ is the gas-phase summation, E_{gas} denotes the gas-phase energy, G_{sol} is the free solvation energy, $T\triangle S$ is the entropy, E_{int} is internal energy, E_{ele} is coulomb and coulomb E_{vdw} is van der Waals energy. E_{gas} was estimated from the AMBER FF14SB forcefield terms. G_{sol} is accounted for by the energy contributions of polar and non-polar states. SA denotes the non-polar solvation energy. G_{SA} was calculated using the solvent-accessible surface area (SASA) obtained by a water probe radius of 1.4 Å. In contrast, the polar solvation, G_{GB}, was obtained by solving the GB expression. S denotes the total entropy of the system, which was calculated using the Normal mode analysis incorporated in AMBERTools and T is the temperature. The interaction entropy ($-T\triangle S$) was estimated using 40 frames due to the computational cost of calculating the change in conformational energy for large frames using the Normal mode method. The surface tension constant, γ, was set at 0.0072 kcal/mol Å^2. Using MM/GBSA method in AMBER 18, per-residue energy decomposition (PRED) at the atomic level was carried out to obtain in quantitative terms the contribution of each residue to the total BFE at the predicted active site.[27,35]

2.4.2. Receptor–Ligand Interactions Systems

The Discovery Studio Visualiser 2020 Client[31] receptor-ligand interaction add-on was utilised to analyse the *pf*LDH active amino acids interaction network with madecassic acid and chloroquine. To identify the molecular forces between the interacting residues and atoms of the ligand, for the madecassic acid- and chloroquine-bound systems, several snapshots were taken at different periods of 300 ns MD trajectories to show their various interactions, which were subsequently visualised using BIOVIA Discovery Studio software.[31] These interactions may provide crucial information to determine if *pf*LDH is a possible target and the contributions of these interactions to the overall design and development of drugs. Interacting residues and the interaction types within the bound systems are elucidated using this software.

2.4.3. Conformational Fluctuations of pfLDH Systems

RMSF analysis estimates the properties of biological molecules in drug design studies, the interactions of protein-protein or protein-ligand at the atomistic level. It indicates the changes in the fluctuations of a protein structure upon binding a ligand.[36] RMSF is the fluctuation of the individual residues of an enzyme or their average position in an obtainable MD simulation trajectory. This analysis provides insights into the flexibility differences in different regions of *pf*LDH enzymes in unbound and bound systems. RMSF is mathematically represented and calculated as follows:

$$sRMSF_i = \frac{\left(RMSF_i - \overline{RMSF}\right)}{\sigma(RMSF)}$$

$RMSF_i$ represents the i^{th} residue RMSF from which the average RMSF is subtracted, which is divided by the standard deviation of the RMSF [σ(RMSF)] to equal to the standardised RMSF [$s(RMSF_i)$].

2.4.4. Radius of Gyration (RoG)

Furthermore, a compactness test was used to investigate the system's stability, in which the RoG of both the unbound and the bound systems was determined. Statistically, the dimensions of biomolecules are predicted using the average radius of gyration (RoG). It describes the atoms' RMSD from a given protein molecule's common center of gravity and shows the molecular compactness of its shape.[37] The compactness of the unbound and bound systems was assessed through 300 ns MD trajectories. The equation below describes how the RoG is determined:

$$r^2gyr = \frac{\left(\sum_{i-1}^{n} W_i(r_i - r^-)^2\right)}{\sum_{i-1}^{n} W_i}$$

The description of the terms shown in the equations is thus; r_i is the i^{th} atom's position, W is each atom's mass, r is the center mass of atom *i*. The mean values were calculated using the RoG values generated throughout times in each trajectory.

2.4.5. Analysis Showing the Per-Residue Energy Decomposition (PRED)

The PRED was performed to estimate the energy contributed by the active site residues to the stability of the lead compound (madecassic acid) relative to *pf*LDH inhibition. The decomposition of the residual

 © 2022 The Authors. Chemistry & Biodiversity Published by Wiley-VHCA AG

energy contribution to binding free energy (BFE) in the protein-ligand complex was analysed by the MM/GBSA method in AMBER18 GPU.

3. Results and Discussion

3.1. Molecular Docking Studies

Previous studies have analysed and revealed two important binding pockets on the *pf*LDH enzymes; the co-factor binding pocket (site A) and the substrate-binding pocket (site B).[7,17] Site A, identified as the NADH binding site, showed as a binding pocket at the N-terminal end of *pf*LDH comprises of amino acid residues: VAL26, GLY27, SER28, GLY29, PHE52, ASP53, ILE54, TYR85, THR97, ALA98, GLY99, PHE100, LYS118, ILE119, GLU122, ILE123, THR139, and ASN140. Site B comprises amino acid residues at the C-terminal end of *pf*LDH, including LYS198, MET199, VAL200, LEU201, GLU226, PHE229, ASP230, VAL233, LYS314, and GLU317. The residues were identified to form binding as the substrate-binding domain. This binding pocket lies on the backside of the active site.[7] The works of Waingeh et al.[7] and Shadrack et al.[17] confirmed that the distribution of docked conformations to the two binding sites was affected by the co-factor presence, where the substrate site was the preferred binding site for ligands when the co-factor was present. Based on preliminary information from the literature, the investigated triterpenes were analysed by docking tool to explore the binding pattern and affinity towards the enzyme. Molecular docking of the compounds by blind docking and site-directed docking into the two active sites (co-factor and substrate) of *pf*LDH were performed.

Lactate dehydrogenase is a glycolytic enzyme that has the potential as a target for developing new drugs because it provides energy to the parasite via glycolysis, and enzyme activity inhibition causes the parasite's death. The co-factor (NADH) and the substrate (pyruvate) are critical factors in the enzyme's activity as *pf*LDH, for parasite survival catalyses the reduction of the keto group in pyruvate to hydroxy with the concomitant oxidation of NADH to NAD^+.[17] Based on this knowledge, we studied the binding of the triterpenes to the two critical pockets of *pf*LDH, for the energetically most favourable binding conformations to be determined.

The investigated triterpenes 19α-hydroxyasiatic acid, arjungenin, 6β,23-dihydroxytormentic acid, combregenin, terminolic acid and madecassic acid had been isolated in our previous work,[21] and they interacted with *pf*LDH with various levels of binding affinity. All six triterpenes occupied the binding sites of the co-factor (NADH) and substrate (pyruvate) of *pf*LDH showing higher binding affinities than chloroquine. The binding affinities of the six triterpenes and chloroquine as standard drug (co-crystallised ligand) is shown in *Table 1*. All dockings were carried out in the absence of NADH.

Based on the favourable energy of interaction, the activity of 19α-hydroxyasiatic acid, arjungenin, 6β,23-dihydroxytormentic acid, combregenin, terminolic acid and madecassic acid showed −7.8, −8.0, −7.7, −7.2, −8.0 and −7.6 Kcal/mol, respectively, all revealing higher binding affinities compared to the standard inhibitor chloroquine (−5.8 Kcal/mol) when docked into the primary site A (*Table 1*). Though, arjungenin and terminolic acid ranked highest among these triterpenes at this site, all compounds showed comparable activity with a strong indication as competitive inhibitors of *pf*LDH at the NADH binding site. On the other side, when docked into the secondary site B, the activity of 19α-hydroxyasiatic acid, arjungenin, 6β,23-dihydroxytormentic acid, combregenin, terminolic acid and madecassic acid showed −8.0, −8.7, −8.1, −7.9, −7.7 and −8.4 Kcal/mol, respectively, all resulting in higher binding affinities compared to chloroquine (−6.0 Kcal/mol). Arjungenin (−8.7 Kcal/mol) showed the highest docking score slightly higher than madecassic acid (−8.4 Kcal/mol). For the blind docking experiment, the activity of 19α-hydroxyasiatic acid, arjungenin, 6β,23-dihydroxytormentic acid, combregenin, terminolic acid and madecassic acid showed −8.0,

Table 1. Binding affinity (kcal/mol) of the investigated triterpenes against *pf*LDH protein target.

Compounds	PubChem ID	Binding energies (kcal/mol)		
		Site A	Site B	Site B*
19α-Hydroxyasiatic acid	N/A	−7.8	−8.0	−8.0
Arjungenin	12444386	−8.0	−8.7	−8.1
6β,23-Dihydroxytormentic acid	N/A	−7.7	−8.1	−8.1
Combregenin	N/A	−7.2	−7.9	−7.9
Terminolic acid	12314613	−8.0	−7.7	−8.1
Madecassic acid	73412	−7.6	−8.4	−8.4
Chloroquine	2719	−5.8	−6.0	−6.0
Oxamate	974	N/A	−4.2	−4.2

* Binding energies of compounds in a blind docking; the compounds preferred binding at the substrate site even in the absence of the NADH co-factor. N/A represents compounds that are not in PubChem but designed on MarvinSketch.

 © 2022 The Authors. Chemistry & Biodiversity Published by Wiley-VHCA AG

−8.1, −8.1, −7.9, −8.1 and −8.4 Kcal/mol, respectively. Premised on the binding energies calculated, using the AutoDock scoring function, the best-docked conformation in each binding site was selected. All ligands studied in this work showed higher binding affinity when docked into site B than site A except for terminolic acid (*Table 1*). Since blind and site-directed docking in this study showed that each ligand has its most probable and energetic binding occurred in site B, it may suggest the most favourable binding site for all the ligand to be the secondary site B. Thus, this seems to indicate an increased frequency and affinity for binding to the substrate-binding site in the absence of bound NADH during docking. These findings are different from the reports by Waingeh *et al.*[7] and Shadrack *et al.*,[17] who stated that site A (co-factor site) showed the best-docked solutions in the absence of the co-factor. The primary reason for this could be a significant structural difference among the compounds investigated in our study (ursane and oleanane triterpenes) and those investigated by Waingeh *et al.*, for instance (quinoline-based compounds). For example, the net charge of the compounds tested in our study is +0, while the quinoline-based compounds in the reference study have a +1 net charge. Also, the degree of complementarity of these two binding sites with the class of compounds in terms of hydrogen bond, van der Waals, steric effect and water networks may contribute to the discrepancies. Thus, this may lead to a difference in the mechanism of binding. However, probing mechanistically into how these structural differences affect the binding conformations in both sites is not within the scope of our study. Although, the binding of co-factor indicated a prospect for competitive inhibition in this study, as the investigated ligands displayed higher binding affinity than the co-crystallised ligand (chloroquine). The ligands displayed comparable binding affinities for both the co-factor and the substrate sites, but the affinities were slightly higher for the substrate-binding site. From the results in *Table 1*, oxamate (a substrate mimic) showed a binding affinity (4.2 kcal/mol) significantly lesser than the test compounds. This finding suggests that the test molecules may modify the enzyme's active site to prevent substrate binding. Hence, this observation indicates allosteric inhibition, where a molecule binds to the allosteric site, thereby causing a shape alteration that reduces the enzyme's affinity for the substrate.[38] It has been shown that *pf*LDH is also functionally dependent on the binding to its substrate to enable a successful catalytic conversion of pyruvate to lactate during glycolysis.[18] Therefore, the findings in this study may be significant because this alternative binding site comprises residues that may interfere with substrate-binding or enzyme's catalytic action.

3.2. Molecular Dynamics (MD) Simulations

The structures and dynamics of biomolecules are valuable information provided by the approach of MD simulations which may contribute to the design of a drug leading to the treatment of malaria. The structural organisation of a protein is a critical defining factor for its biological activity; hence, there could be either a positive or negative effect on the activities of such protein when there are considerable alterations in its structural integrity.[39,40] This phenomenon is fundamental in the molecular mechanism of druggable molecules when they are utilised to treat disease to target specific pathogenic macromolecules (proteins, for example) that drive the progression of the disease. Moreover, in consistence with the basis of this study, it was imperative to offer relevant information related to the allosteric inhibitory potential of CQ and MA towards *pf*LDH, a vital malaria target. In this study, the MA-bound system showed a considerable high binding affinity with more hydrogen bond interaction than the other ligand-bounds when docked at the substrate-binding site. Also, in our previous work, where alongside other compounds, its antiplasmodial effect was tested against both chloroquine-sensitive (D10) and -resistant strains (W2) of the malarial parasite, MA had shown the highest activity (D10: 28 ± 12 μg/mL, W2: 17 ± 4 μg/mL) compared to others. As a result of this promising effect, madecassic acid-bound, chloroquine-bound and the unbound *pf*LDH systems were subjected to 300 ns MD simulations to analyse the energetics of each complex and check the convergence of dynamic stability. Trajectories produced from the complexes simulated were further analysed for C-α atom RMSD and C-α RMSF to gain insights into the structural dynamics and equilibrium upon binding. The C-α RoG, PRED, dynamic cross-correlation matrix (DCCM), and defined secondary structure protein (DSSP) were also analysed.

3.3. Root Mean Square Deviation (RMSD)

RMSD was used to determine the system convergence and structural stability of the three systems under our investigation, wherein as a result of the atomistic deviations, the conformational changes were estimated using the C-α backbone RMSD. Long time MD

 © 2022 The Authors. Chemistry & Biodiversity Published by Wiley-VHCA AG

simulations are required for a protein system to attain stability. The stability of *pf*LDH upon binding of MA and CQ was examined by calculating the deviation of C-α atoms throughout the simulation.[41] An increase in RMSD value is indicative of more atomistic deviation, suggesting a protein with an unstable structure, while a system with a low RMSD value suggests a protein with a reduced structural deviation, hence highly stable.[42,43] As shown from *Figure 3B*, the estimated average RMSD values were 1.60 Å, 2.00 Å, and 1.62 Å for MA-bound, CQ-bound, and unbound systems, respectively. The results showed that all

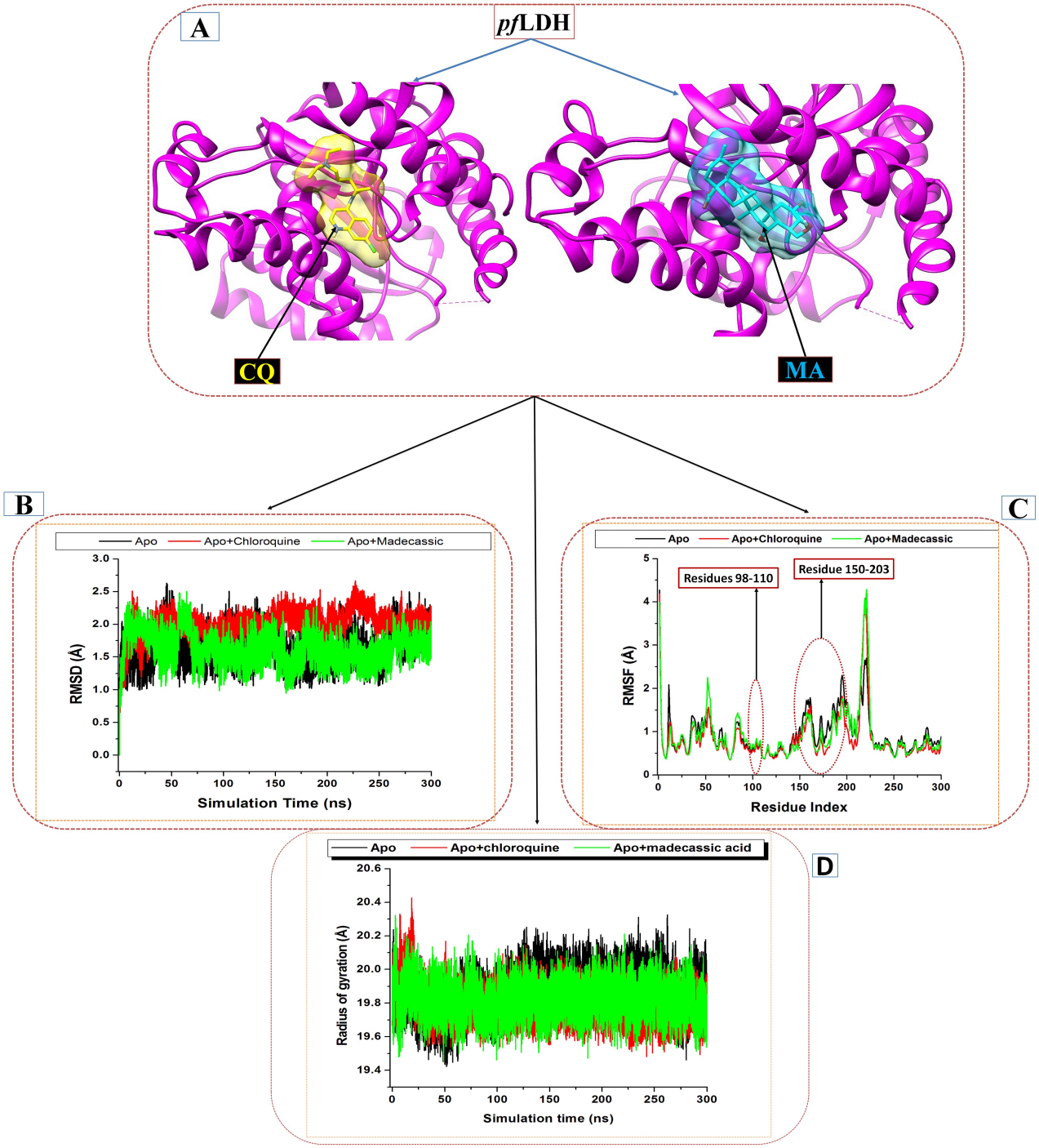

Figure 3. (A) Chloroquine (grey) and madecassic acid (cyan) bound to the *pf*LDH substrate binding site. C-α backbone (B) RMSD, (C) RMSF and (D) RoG plots of Apo and bound systems ran for 300 ns MD simulation.

 © 2022 The Authors. Chemistry & Biodiversity Published by Wiley-VHCA AG

simulated systems displayed an average RMSD up to 2 Å at maximum, signifying a comparatively stable simulation. Likewise, all the systems achieved convergence almost throughout the entire 300 ns simulation time. The RMSD results showed that the binding of MA had a more stabilising effect on the binding domain than CQ and unbound-conformation. The highly stable binding pocket residues observed in MA-bound could have favoured a steadier residue interaction with MA and possibly stronger binding to *pf*LDH relative to CQ.

3.4. Root Mean Square Fluctuation (RMSF)

Through the RMSF, we gain insight into the flexibility of the protein's structure by estimating the fluctuation of each amino acid present in the protein.[42,44] The conformational dynamics of these amino acids, which form part of the building blocks of the protein, play a critical role in the overall function of the protein.[45] The RMSF analysis provides a better understanding of the changes in conformation upon ligand binding and shows the significance of molecular dynamics at the atomistic level. The MD simulations trajectories in obtaining the RMSF reveal the differences in the residues' flexibilities with or without a ligand.[29] So, we calculated the RMSF of the amino acids that constitute *pf*LDH upon binding of CQ and MA to monitor their impact on the conformational dynamics. The higher RMSF values indicate more flexible movements, while the lower fluctuation values show lesser conformational changes during the simulation. The average RMSF values of Apo, ApoCQ, and ApoMA systems were 0.94 Å, 0.83 Å, and 0.92 Å, respectively (*Figure 3C*). As shown, the unbound *pf*LDH showed the highest residue fluctuation relative to CQ and MA, indicating that the fluctuation of *pf*LDH reduced upon the binding of CQ and MA. Moreover, the lower RMSF value for both CQ and MA compared to the Apo system may indicate the system's compactness. The mobile loop closure, comprising surface-residues 98–110, is one of the major substrate-binding pathways in LDH catalysis.[7,16] Dynamic fluctuations are essential to enable the accessibility of substrate to the active site since the enzyme's active site lies deep into the protein structure.[20] Thus, the low molecular fluctuation recorded for the bound-systems within residues 98–110 region may indicate the lack of substrate accessibility to the active site, thereby preventing the necessary protein structural changes leading to the activation of pyruvate and NADH for catalysis. This observation could indicate inhibitory effects for the ligands. In LDH, the mobile loop is in open conformation before ligand binding and closes over the active site after binding substrate. These open and close transitions involve a temporary structural change of about 10%–15% within the substrate-binding region, which is required to move amino acid residues necessary in catalysis into closeness with the bound substrate.[7,16] The molecules we investigated in this work are bound at or close to the active site, and since their binding affinity is higher than that of oxamate, it is thus plausible to consider them as competitive inhibitors of the substrate. On the other side, the identified substrate-site binding may also interfere with the structural changes observed in mobile-loop motion and are vital in substrate binding. Thus, loop movements inhibition may be enabled by significant interactions formed with residues such as LYS198, MET199, LEU201, which are within the substrate-binding domain and close to the active site. Thus, the Apo system showed elevated C-α atoms fluctuations above CQ and MA in the region comprised of residues 150–203, which correspond to the LYS198, MET199, and LEU201 interacting residues.

3.5. Radius of Gyration (RoG)

RoG measures the compactness of the entire protein structure throughout the simulation. The tightness or looseness of the structure of a protein is capable of interfering with its physiological properties. The work of Akher et al.[40] emphasised the interplay between C-α RoG and compactness of protein structure, where they showed that loss in structural compactness is due to a high RoG value, and structurally compact protein is due to a low RoG value. We, therefore, estimated the effects of binding of CQ and MA on the compactness of the active site across the time of MD simulations. The average RoG values of Apo, ApoCQ, and ApoMA systems were 19.87 Å, 19.80 Å, and 19.82 Å, respectively (*Figure 3D*), showing very similar compactness for the three systems. However, the results revealed the atomic distributions in Apo from 125–300 ns to indicate high RoG and low compactness, which is correlative with the high RMSF observed between residues 150–203 and 240–305. The lower RoG in these regions for the bound-systems implied that the binding of CQ and MA resulted in a tighter *pf*LDH conformation relative to the unbound system.

 © 2022 The Authors. Chemistry & Biodiversity Published by Wiley-VHCA AG

3.6. Comparative Binding Free Energy Profile

Thermodynamic calculations were performed to get insights quantitatively into the mechanistic binding profiles of CQ and MA towards *pf*LDH using the MM/GBSA approach.[26] The MM/GBSA method is a reliable approach frequently used to estimate the binding free energy (BFE) of a small molecule to a protein and has become a very useful *in silico* methods for assessing binding affinity. Evaluating the binding affinities of CQ and MA could help insight into the reason for the perceived competitive advantage of MA over CQ and its ultimate contribution to the inhibition of *pf*LDH function. The computation of the binding affinity of an inhibitor to a protein is done using trajectory or snapshots of the complex through which we understand how both inhibitors CQ and MA bind to *pf*LDH. We calculated the BFE and per-residue decomposition of each compound at the substrate-binding site of the enzyme to ascertain the binding affinity of the compounds and to establish the basis of potential inhibition against *pf*LDH. The calculated binding free energies of both CQ and MA are shown in *Table 2*. CQ and MA exhibited comparably high total free binding energy of −25.28 kcal/mol and −33.40 kcal/mol, respectively, towards *pf*LDH. The BFE provides distinct energy contributions within the binding pockets and the binding conformations that present the best intermolecular interactions at the active sites of the protein.[29] Therefore, the observed high BFE could be due to the increased electrostatic energy and van der Waals recorded in the calculations and could account for the inhibition by both compounds. The total BFE value was increasingly more in the MA-bound system compared to the CQ-bound system. This observation demonstrates that MA exhibited more potent inhibition of and higher binding affinity to *pf*LDH when compared to CQ. The MM/GBSA method has been applicable in reproducing and rationalising experimental findings and expanding on results from virtual screening and docking calculations.[34,35] The results agreed with the above-presented molecular docking analysis. The interaction of the inhibitor with residues induced ligand's stabilisation in the target site, which led to its inhibitory activity.

3.7. Per-Residue Energy Decomposition (PRED) and Ligand Interactions with pfLDH

The RMSD calculations showed that the simulated complexes had excellent stability throughout the 300 ns of simulation. The stabilised conformation gives a chance for favourable interactions, which could have affected the binding affinity of the inhibitors to *pf*LDH. The PRED showed the molecular interactions between the ligands and interacting residues.[26] To further establish the structure-binding affinity relationship between the ligands and *pf*LDH, the contribution of energy by residues of *pf*LDH binding pocket towards the binding of CQ and MA was quantitatively evaluated. This PRED calculation revealed crucial interacting residues and their contribution to the binding affinity of CQ and MA. We obtained the energy contributions by individual active site residues involved in the binding and stability of both compounds by further decomposition of the total binding protein energy (BPE) using the MM/GBSA approach. Most of the binding pocket residues contributed strongly to the interactions through van der Waals and electrostatic forces (*Figures 4* and *5*). These two forces revealed the residue and energy that showed significant influence on the total binding energy. *Figures 4C* and *5* C, respectively, showed the per-residue decomposition of *pf*LDH-CQ and *pf*LDH-MA. The extent of stability and the binding strength of the two complexes at the binding site is dependent on the intermolecular forces that occurred between the inhibitor and the residues at the active site.

For the *pf*LDH-CQ system, the interacting residues and the most energy contributions towards the complex are: VAL176 (−1.89 kcal/mol), LEU177 (−1.62 kcal/mol), ASP200 (0.12 kcal/mol), PHE207 (−2.26 kcal/mol), VAL211 (−0.44 kcal/mol) and LYS290 (−0.83 kcal/mol). Each residue contributed high energy towards the complex, but ASP200 contributed lower total energy, which could be unfavourable in CQ binding and stability, though it showed the highest

Table 2. Thermodynamics analysis of CQ-*pf*LDH and MA-*pf*LDH interactions: MM/GBSA-based binding free energy contributions to the ligands.

Complex	Energy components (kcal/mol)					
	$\triangle E_{vdw}$	$\triangle E_{ele}$	$\triangle G_{gas}$	$\triangle G_{GB}$	G_{solv}	$\triangle G_{bind}$
Apo-CQ	−29.8311	−78.0310	−107.8621	86.3434	82.5799	−25.2822
Apo-MA	−38.6366	−28.5699	−67.2064	38.9456	33.8078	−33.3986

 © 2022 The Authors. Chemistry & Biodiversity Published by Wiley-VHCA AG

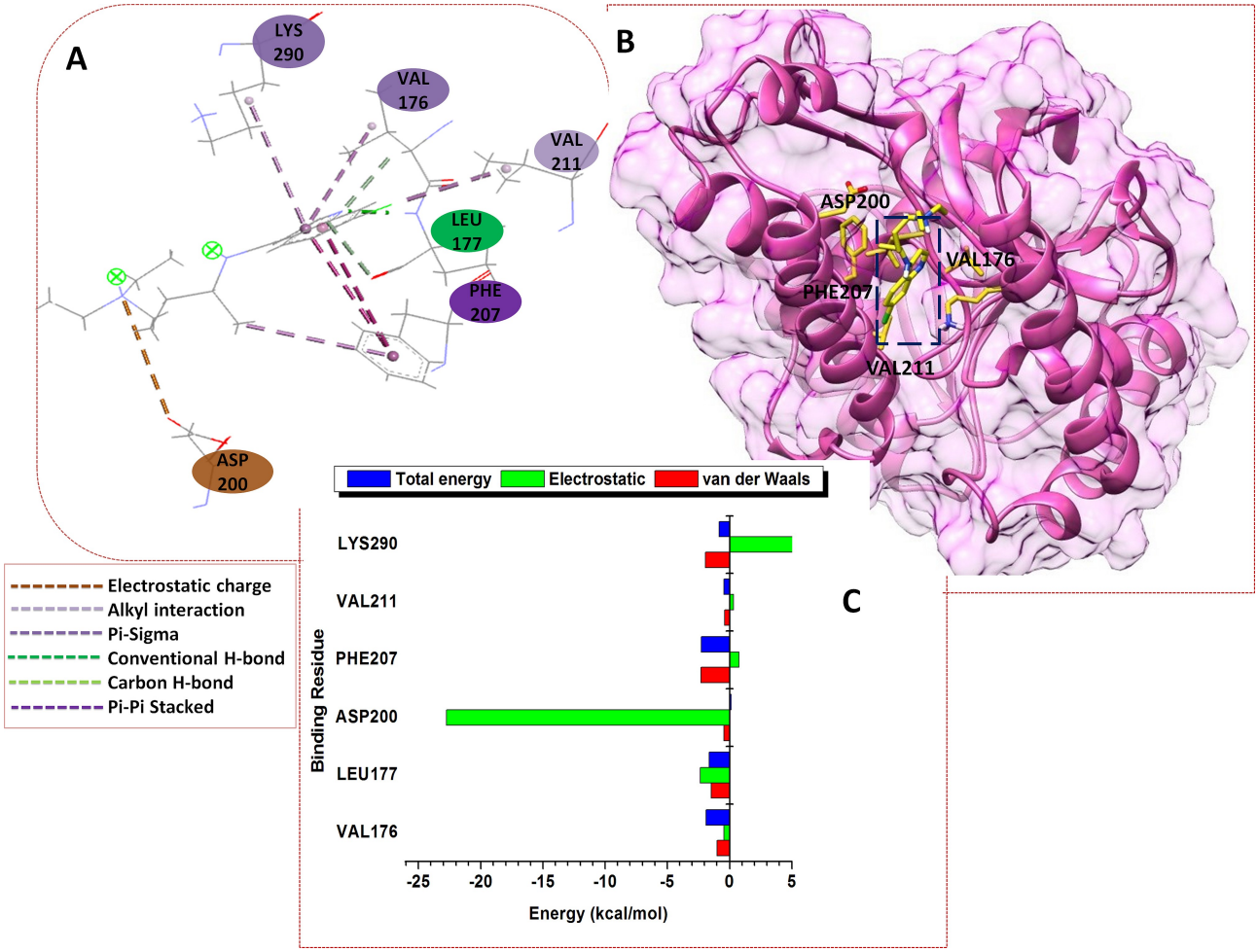

Figure 4. (A) A visualisation of the chloroquine-*pf*LDH interaction network. (B) 3D structure of chloroquine bound to the *pf*LDH active site. (C) Energy contributions of the interacting residues of *pf*LDH with chloroquine.

electrostatic interaction (−22.77 kcal/mol). However, PHE207 (−2.30 kcal/mol) and LYS290 (−1.92 kcal/mol) have the highest van der Waals (vdW) energy contributions to the binding of the inhibitor. The residues that contributed higher energies towards the complex and the per-residue interaction energy of the *pf*LDH-MA system include LYS174 (−0.64 kcal/mol), MET175 (−1.32 kcal/mol), LEU177 (−1.37 kcal/mol), LYS179 (−1.56 kcal/mol), PHE207 (−1.81 kcal/mol), VAL211 (−1.26 kcal/mol) and LYS290 (−1.25 kcal/mol). All interacting residues recorded in *pf*LDH-MA contributed high energy towards the complex, but PHE207 accounted for the highest total energy, a similar observation in the *pf*LDH-CQ system. Based on these results, LYS290 (−1.97 kcal/mol), LEU177 (−1.90 kcal/mol), and PHE207 (−1.79 kcal/mol) have the highest vdW energy contributions to the binding of MA towards *pf*LDH. Therefore, the vdW interactions due to residues 290, 211, 207, 179, 177 and 174 and the electrostatic interactions due to LYS179 (−7.18 kcal/mol), MET175 (−2.41 kcal/mol) and LYS174 (−1.99 kcal/mol) contributed to the higher stable system of *pf*LDH-MA ($\triangle G_{bind} = -33.40$ kcal/mol) relative to *pf*LDH-CQ ($\triangle G_{bind} = -25.28$ kcal/mol). The $\triangle G_{bind}$ for the *pf*LDH-MA system showed madecassic acid as highly stable. The interactions between the hydrophobic active site residue enhance the binding and stability of MA in the pocket. Hence, these strong and stable interactions between MA and *pf*LDH greatly influence its inhibitory potential. These findings can be useful in the potential identification of antimalarial compounds in the future study of the *pf*LDH protein as a target.

The favourable orientation of the ligands' functional groups such as electronegative chlorine, $-C_6H_5$ and $-C_5H_5N$ for CQ and –OH, C=O for MA interacted

 © 2022 The Authors. Chemistry & Biodiversity Published by Wiley-VHCA AG

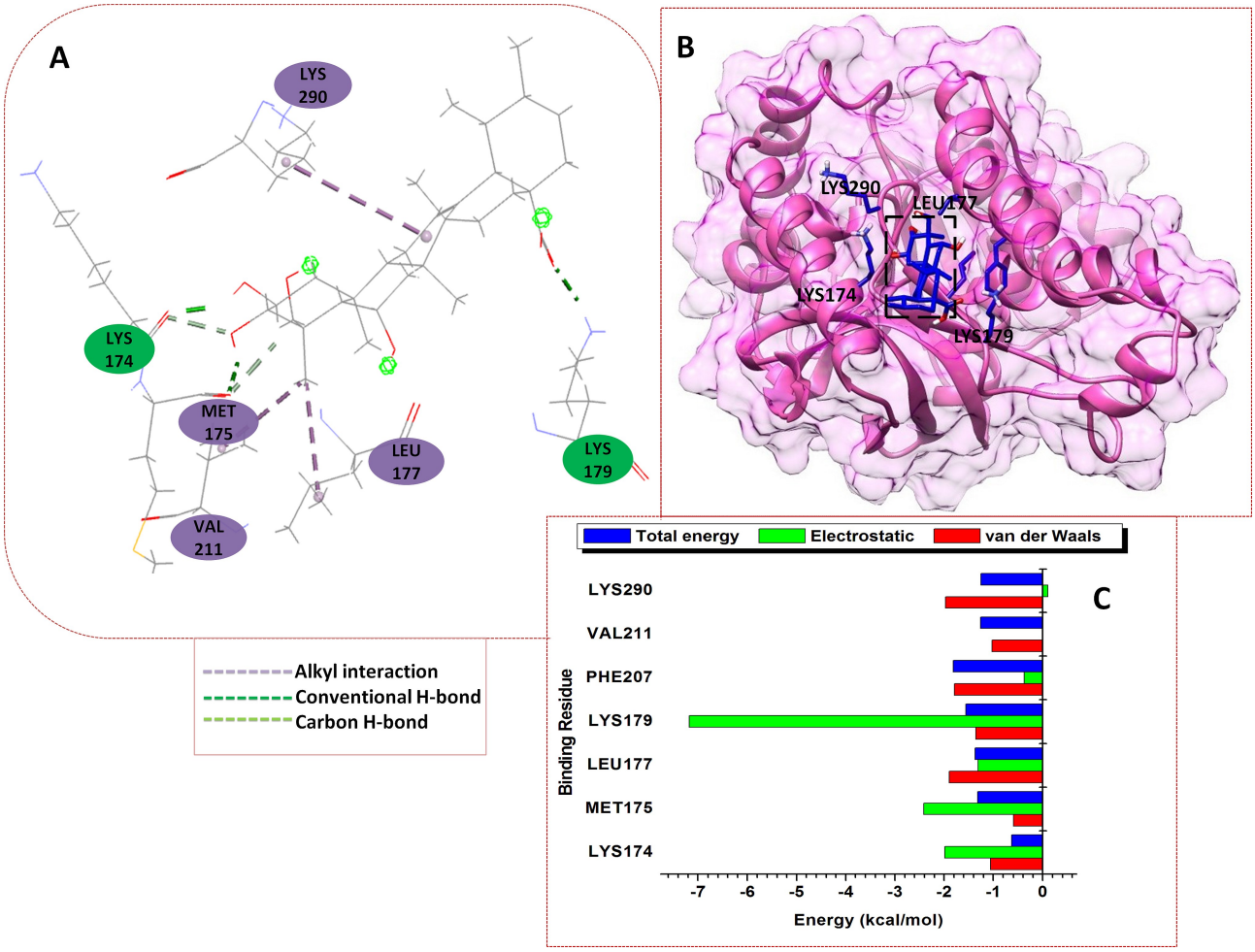

Figure 5. (A) A visualisation of the madecassic acid-*pf*LDH interaction network. (B) 3D structure of madecassic acid bound to the *pf*LDH active site. (C) Energy contributions of the interacting residues of *pf*LDH with madecassic acid.

with the favourable groups at the active site residue such as $-NH_2$, –COOH, which formed strong bonds. In the interactions of *pf*LDH, the methyl C-atoms of the side chains of VAL211 developed an alkyl hydrophobic bond with the highly electronegative chlorine. Also, a conventional hydrogen bond was formed in which the backbone H-atom of LEU177 bonded with N at position 4. The resonating rings (C1-C3 and C5-C10) of CQ formed the strong pi-hydrophobic solid bonds with the phenyl ring of PHE207. Similarly, the methyl C-atoms of the side chains of VAL176 and LYS290 formed stable and strong pi-sigma bonds with the pyridine (C_5H_5N) ring. The O-atom of the carboxy of ASP200 showed a strong, attractive charge towards diethyl nitrogen (N-17).

There were mainly hydrogen bonds and alkyl hydrophobic interactions formed in the *pf*LDH-MA system. The methyl C-atom of the side chain of LYS290 developed a stable alkyl hydrophobic bond with the methyl C-atom of the prenyl group in MA (*Figure 5A*). Also, the methyl C-atoms of the side chains of LEU177 and VAL211 formed strong alkyl hydrophobic bonds with the methyl C-atom at position 4 and the H-atom of the methyl group. Other observed interactions are the conventional hydrogen bonds formed from the carboxy O of LYS174 and MET175 with H-atoms of OH groups at positions 2 and 3, respectively. The H-atom of the amide group in LYS179 formed a conventional H-bond with the carboxy O at position 28. Non-classical H-bond is formed between the carboxy O-atom of MET175 and the methine hydrogen (H-1). The same H-bond was formed between the backbone H-atom of LYS174 bonded with the O-atom of the oxymethylene group at position 2 were formed.

 © 2022 The Authors. Chemistry & Biodiversity Published by Wiley-VHCA AG

3.8. Dynamic Cross-Correlation Matrix (DCCM)

During the 300 ns MD simulations, the DCCM was analysed to obtain the position of the C-α atoms of the bound and unbound systems.[29,41] Considering the different inhibitory activities of MA and CQ, this analysis was done further to study the inter-residual dynamics and motions of *pf*LDH. With this, the motions that represent correlation (positive) and anti-correlation (negative) of constituent residues around their C-α atoms were determined across the MD simulation period. The C-α atoms motions are shown in *Figure 6* (A–C), indicating highly positive correlated motions (deep red to yellow), highly negative anti-correlated movements (cyan to black) and similar correlations (green). The positive correlation of motions was most notable in *pf*LDH unbound system, followed by the MA-bound, and least in the CQ-bound (*Figure 6*). The regions that constitute the active site reflect mainly the pattern of motions. It can be inferred from the plot that upon binding of MA (*Figure 6C*), the residues of the regions of the active site (150-210) showed an increased positive relationship which indicates a high degree of fluctuation and a high average RMSF value in comparison to CQ-bound (*Figure 6B*). These results correlated with the average RMSF findings where the MA-bound system was more fluctuated than the CQ-bound. Additionally, this

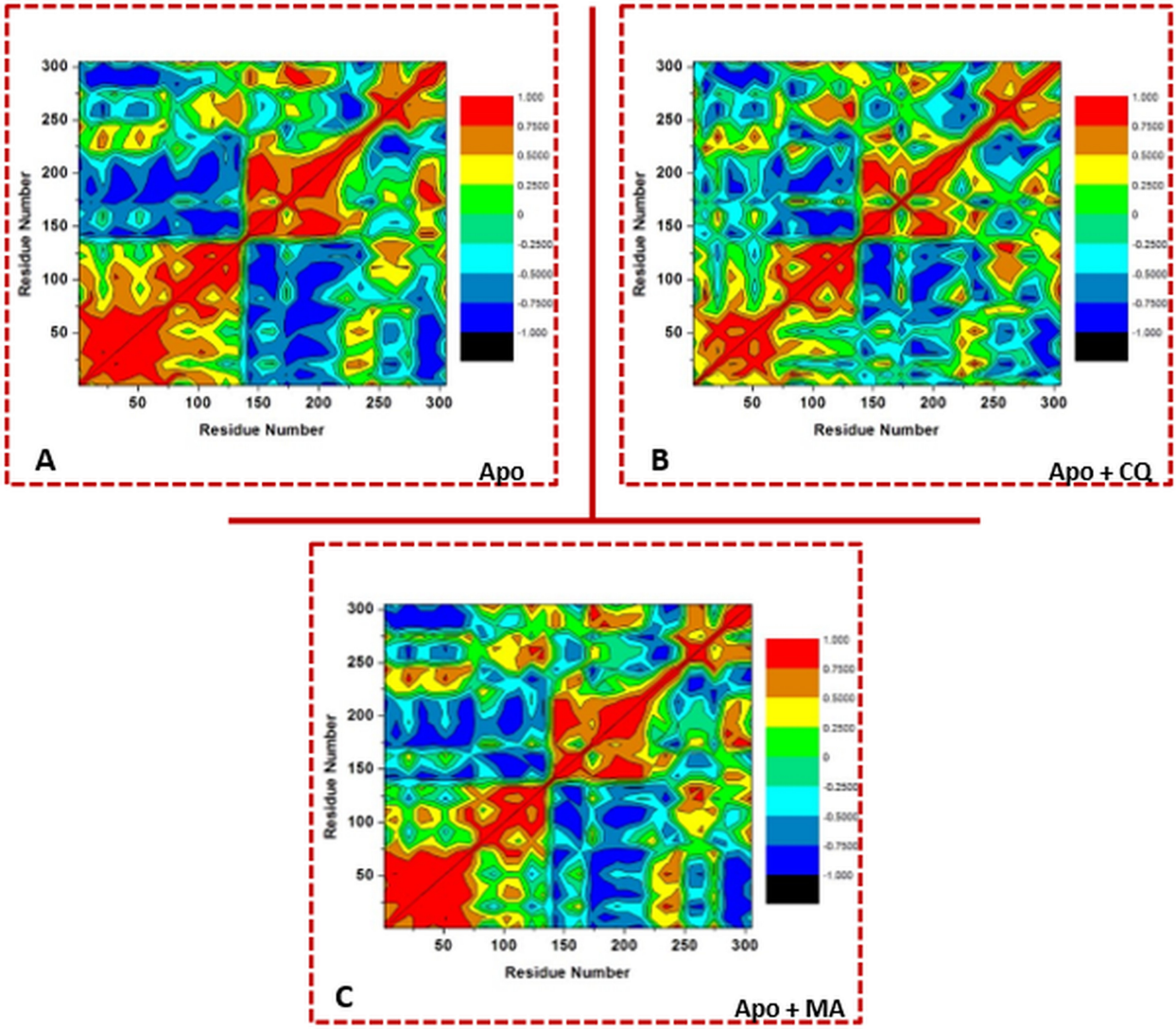

Figure 6. Dynamic cross-correlation matrix showing the correlations of residues in the Apo (A), chloroquine-bound *pf*LDH system (B) and madecassic acid-bound *pf*LDH system (C). The colored legends on the right hand of each plot indicate the status of correlated motions.

 © 2022 The Authors. Chemistry & Biodiversity Published by Wiley-VHCA AG

observed correlation of motions at the regions of the active site could as well correspond with the lower compactness shown by the RoG results.

3.9. Defined Secondary Structure Protein (DSSP)

DSSP was analysed to characterise protein elements, including loops, α-helices, β-sheets and coils, which do not unfold directly or adequately.[46] This analysis provided further insights into the inhibitory activity of CQ-bound and MA-bound against the *pf*LDH catalytic functions using the 300 ns trajectories obtained during MD simulations. The DSSP element assignors used in this work are None, Para, Anti, 3–10, Alpha, Turn and Bend, which are indicated as legends on the far righthand side of each chart. Using these, we monitored the protein's visual transition or unfolding behaviour upon ligand binding compared with free *pf*LDH. *Figure 7* (A–C) shows the DSSP plots for the unbound (A), CQ-bound system (B) and MA-bound system (C). The unbound *pf*LDH, the CQ-bound and MA-bound DSSP plots showed no significant conformational transformations in their secondary structure elements. However, around 170–175 in the CQ-bound system were transitioning to Bend during 280 to 300 ns. At the same residue regions, from 210 to 215 ns, residues transitioned from Bend to Anti in the MA-bound system. Also, both CQ- and MA-bound systems were transitioned to Bend in the same regions of residues 170–175 between 80 and 82 ns.

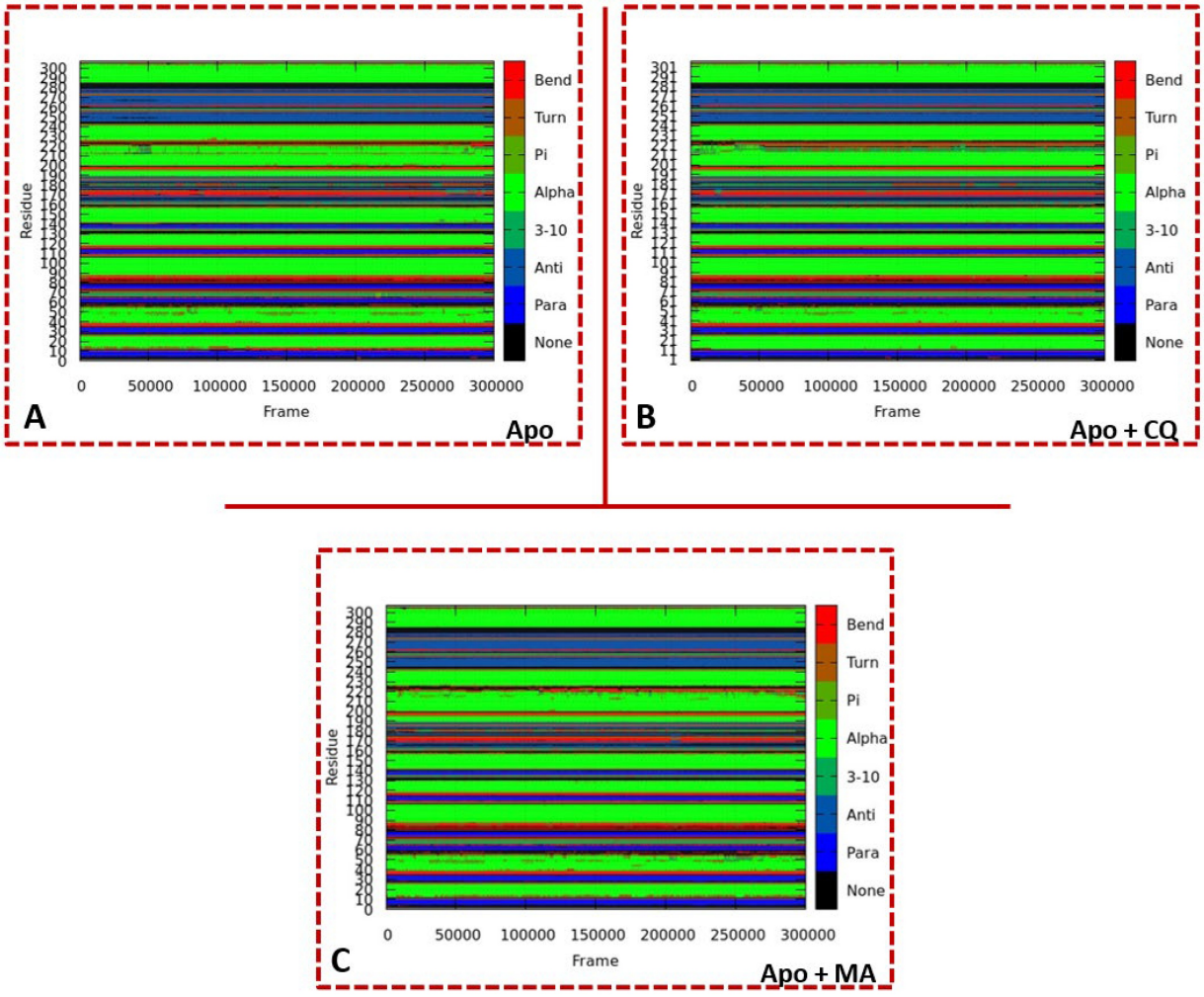

Figure 7. The DSSP charts for *pf*LDH protein systems, (A) unbound *pf*LDH, (B) chloroquine bound *pf*LDH and (C) madecassic acid bound *pf*LDH, taken throughout 300 ns MD simulations.

 © 2022 The Authors. Chemistry & Biodiversity Published by Wiley-VHCA AG

3.10. Structural Dynamics of the Loop Carrying Active Site Residues in pfLDH Protein and Distance Metrics

Perturbed dynamical properties or conformational changes at sites that are spatially distant to a site where a modification or binding takes place are essential components that relate allostery to protein function. These motions with their complexities should therefore be studied.[47] The study of loops provides valuable information to help determine the protein function, such as dynamics, shape and ligand binding. They serve as the connecting ends for the secondary structure (α-helices and β-strand) and function in protein-protein interaction, protein-ligand interaction, and enzyme catalysis.[27] This study identified a vital loop located around the substrate site, which can exist in a closed and open conformation; therefore, we determined its role in the *pf*LDH conformation and ligand binding. This functional loop in the substrate-binding domain contains residues 158–188 (red) as shown in *Figure 8*, which illustrates the trajectory images of the Apo, CQ-bound and MA-bound systems at 0, 100, 200 and 300 ns MD simulations. These findings helped to visualise the magnitude of structural changes within these systems at the different simulation times. This loop is crucial in binding the ligand MA because it contains the three most contributing interacting residues, which include LYS174, MET175 and LEU177 of the active site. *Figure 8* revealed significant conformational changes in this loop in the Apo, CQ-bound and MA-bound structures as the simulation time increases from 0 to 300 ns. Two observable changes occurred in the Apo, CQ-bound and MA-bound systems, where the loop exhibited twisting and transitions at different MD simulation times. Two significant portions on the loop were identified and studied for their conformational changes; the part with residues 160–162 (enclosed in purple oval shape) and the portion with residues 172–185 (enclosed in black oval shape). At 100 ns MD simulation, the changes in Apo were due to structural transition of the region of residues 160–162 to a helix, and the region enclosed in black oval shape (residues 172–180) twisted and shifted away from the active site of *pf*LDH. Simultaneously, the CQ-bound showed transitions into β-strand (yellow oval shape) and helix (black oval shape) in the regions of residues 175–177 and 179–180, respectively. In the MA-bound, there was an extension with a structural transition into a helix (residues 179–185), while interacting residues 174–177 region (yellow oval shape) did not undergo a conformational change. At 200 ns, the conformational changes, transitions into helices in both regions of residues 160–162 and 179–181, occurred in only Apo and MA-bound systems. Moreover, conformational changes occurred at 300 ns in Apo (structural transition into helix at region 160–162 and twisting at the region of residue 179–181), CQ-bound (structural transition into helix at region 179–181) and MA-bound (structural transitions into helix at regions 160–162 and 179–181).

From the trajectory snapshots of the 300 ns MD simulations, the analysis of distance (D) was determined for Apo and MA-bound systems to gain further insights into the inhibitory potency of MA on the dynamical conformation and movements of *pf*LDH. Measuring D between the side chains of two different interacting residues is a commonly used metric for describing proteins' curling and twisting motions.[30] Thus, the distance between loop residues MET175 and LEU177 around the active site, responsible for the opened and closed structure conformations, was considered in this study. The distances between these interacting residues of the bound and unbound *pf*LDH were determined at 0, 150, and 300 ns. The two residues showed an in-between distance in the unbound *pf*LDH was 7.405 Å at 0 ns and increased to 8.45 Å after 150 ns and 8.61 Å after 300 ns (*Figure 9* A, C and E). The in-between distance of the two residues in the MA-bound system was 7.405 Å at 0 ns, increased to 7.93 Å after 150 ns, and decreased to 6.019 Å after 300 ns (*Figure 9* B, D and F). The distance between the two residues was reduced during the MD simulation time in the MA-bound *pf*LDH system. The interactions and stability of the MA-bound *pf*LDH system are enhanced by this decrease in the distance. Thus, stronger interactions between MA and the interacting residues at the active site result from the decrease in the distance, therefore enhancing effective inhibition of the catalytic activity of *pf*LDH enzyme.

4. Conclusion

In this study, an investigation of the binding of six triterpene-based ligands to *Plasmodium falciparum* lactate dehydrogenase was carried out using molecular docking virtual screening tools. Our study outcomes showed that the molecules were effectively bound to the enzyme at both the co-factor and the substrate-binding sites through site-directed docking but bound to only the substrate-binding site by blind docking. It was observed that the compounds were bound to the co-factor binding pocket of *pf*LDH. Thus,

 © 2022 The Authors. Chemistry & Biodiversity Published by Wiley-VHCA AG

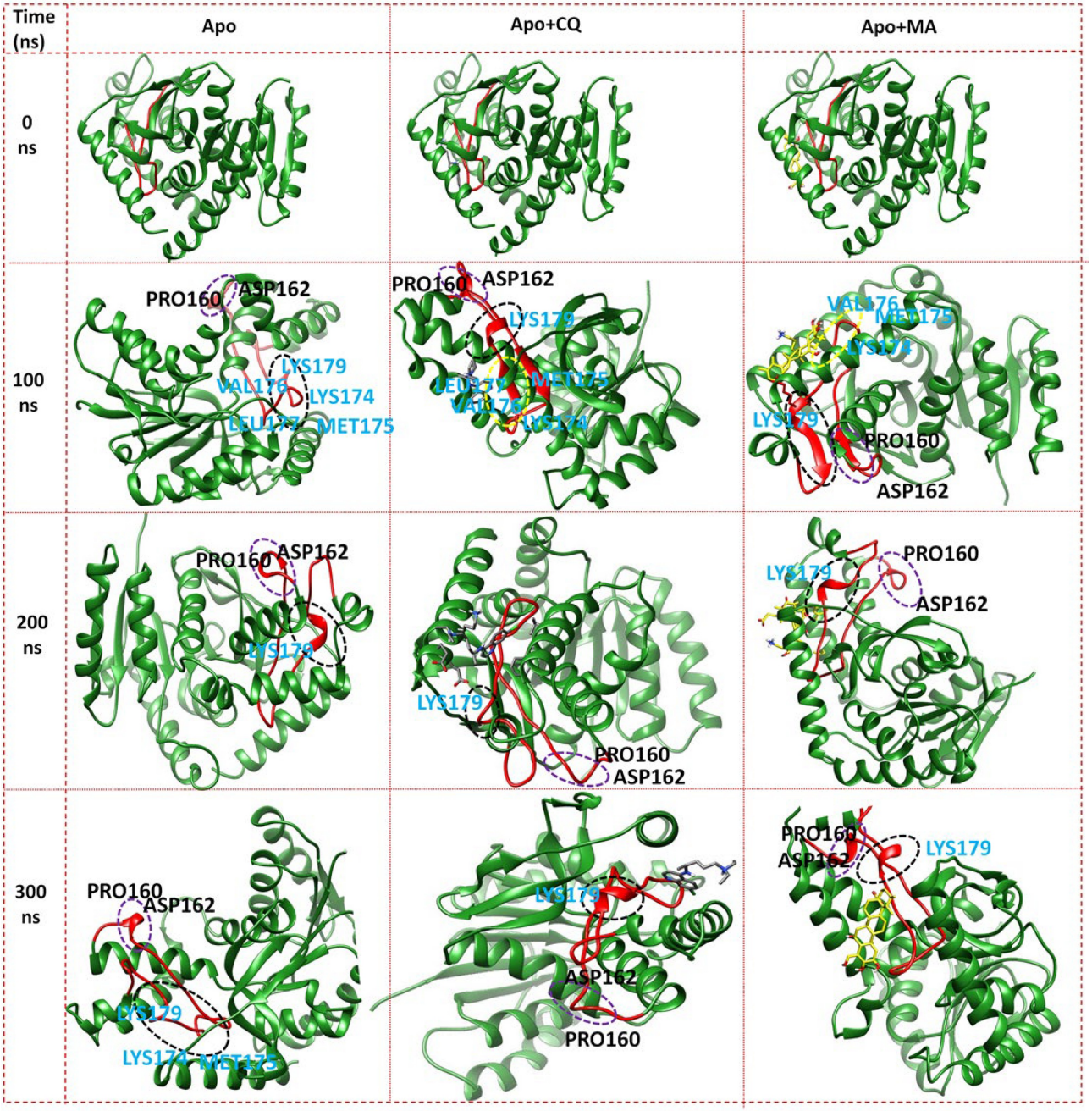

Figure 8. Trajectory snapshots representing the degree of structural changes at the loop carrying the active site residues between Apo, *pf*LDH-CQ and *pf*LDH-MA at 0, 100, 200 and 300 ns.

all of the investigated triterpenes may be potential competitive inhibitors of the co-factor, since all had a binding affinity higher than chloroquine, a previously reported competitive inhibitor. However, molecular docking (through blind docking) also identified a secondary binding site. The molecules bound to this site resulted in higher binding affinities than the co-factor site, which indicates a non-competitive inhibitory potential. This alternative binding site comprises substrate-binding domain amino acid residues and suggests a potential to interfere with substrate-binding or catalytic function by inhibition of *pf*LDH enzyme catalysis.

Moreover, studying the molecular mechanism of *pf*LDH and the mode of action of madecassic acid using a panel of computational tools provides a novel

 © 2022 The Authors. Chemistry & Biodiversity Published by Wiley-VHCA AG

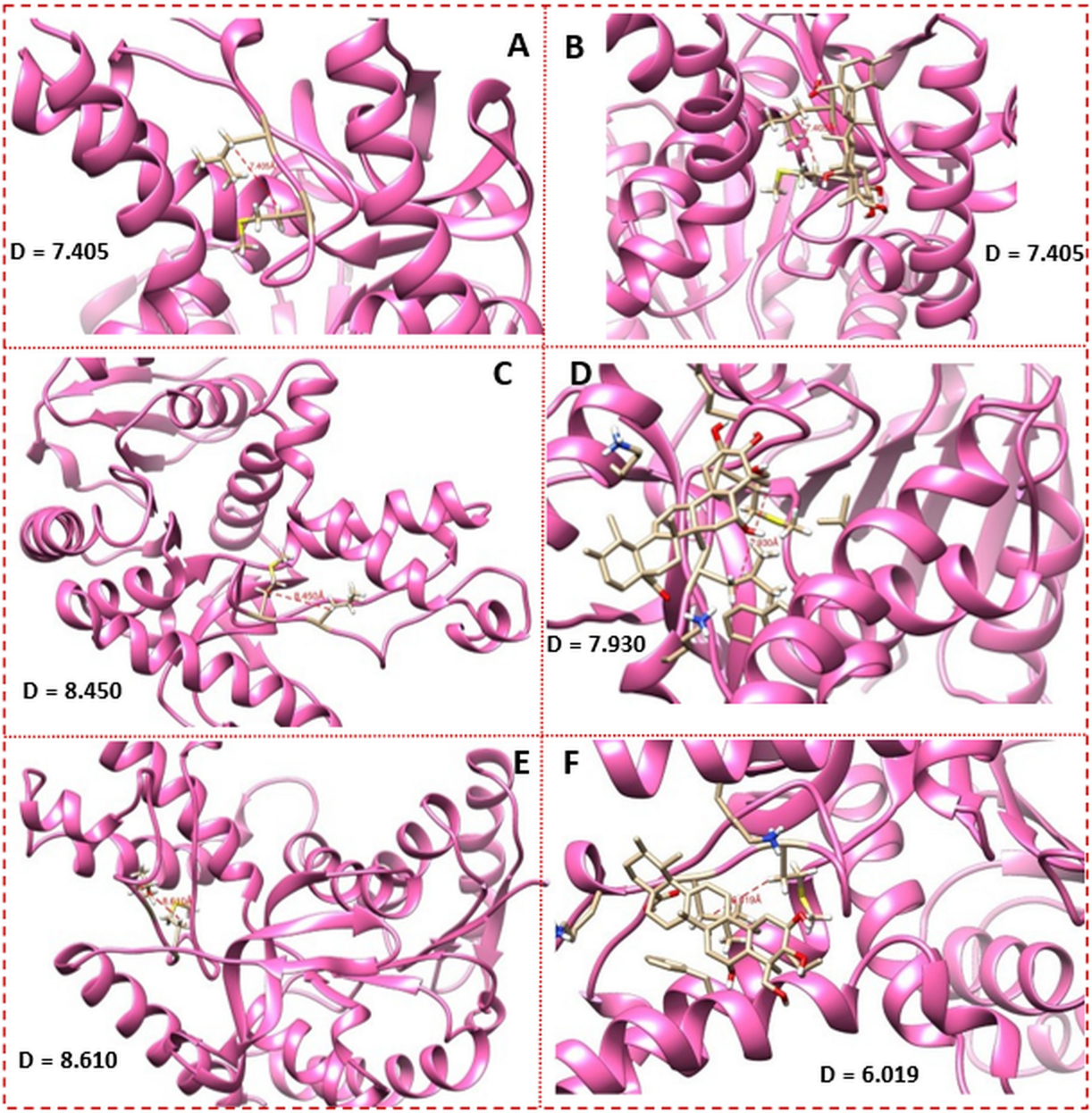

Figure 9. Distance (D) between MET175 and LEU177 of the unbound and MA-bound *pf*LDH, measured using the snapshots taken at 0, 150 and 300 ns MD simulations.

approach to designing new antimalarial drugs. According to our findings, all systems simulated showed an average RMSD less than 2 Å indicating a relatively stable simulation and well-equilibrated systems throughout the simulation time. The RMSD results showed the binding of MA to result in a more substantial stabilising effect on the binding domain relative to CQ and the unbound-*pf*LDH. The highly stable binding pocket residues observed in MA-bound could have favoured a steadier residue interaction with MA and possibly stronger binding to *pf*LDH relative to CQ. The total binding free energy is higher in the MA-bound system than in the CQ-bound system. This observation demonstrates that MA exhibited stronger inhibition of *pf*LDH when compared to CQ. Therefore, this explains that MA is a compound with a higher binding affinity toward *pf*LDH than CQ. The $\triangle G_{bind}$ for the *pf*LDH-MA system showed madecassic acid as highly stable. The interactions between the hydrophobic active site residue enhance the

 © 2022 The Authors. Chemistry & Biodiversity Published by Wiley-VHCA AG

binding and stability of MA in the pocket. Hence, the strong and stable interactions between MA and *pf*LDH have a high inhibitory potential. The vital loop in the substrate-binding domain, which is instrumental in binding MA-*pf*LDH bound, was identified. Thus, the loop conformational changes due to binding of the ligand provide essential information on how MA could inhibit the protein function. These findings provide a platform for the potential identification of antimalarial compounds in the future study of *pf*LDH protein as a target. Our findings reported here help us understand the structural and dynamic behaviour of *pf*LDH protein and its interactions with the inhibitor, which could assist in a further experimental study. It is also recommended that a laboratory experiment further validate the allostery function of this secondary binding site for its potential in inhibiting the activity of *pf*LDH.

Compliance with Ethical Standards

Ethical Approval

This article does not contain any studies with human participants or animals performed by any of the authors.

Research involving Human Participants and/or Animals

Informed Consent

This study did not require informed consent since the study does not contain any studies with human participants performed by any of the authors.

Funding

No funding was received for this study

Acknowledgment

First, the authors acknowledge THE ALMIGHTY GOD, who created all things, including lives, wisdom, and knowledge, for every human being. Second, we acknowledge the Centre for High-Performance Computing (CHPC), Cape-Town for computational resources, and the University of KwaZulu-Natal, Durban, South Africa.

Conflict of Interest

The authors declare no conflict of interest.

Author Contribution Statement

WM Oluyemi and BB Samuel conceptualised the research ideas; WM Oluyemi and AT Adewumi designed, conducted the research investigation and analysed the data; WM Oluyemi and YA Adekunle wrote the main draft of the manuscript; AT Adewumi, BB Samuel, MES Soliman and L Krenn supervised the research project and did the reviewing and editing of the manuscript.

References

[1] S. Saxena, L. Durgam, L. Guruprasad, 'Multiple e-Pharmacophore Modelling Pooled with High-Throughput Virtual Screening, Docking and Molecular dynamics simulations to Discover Potential Inhibitor of *Plasmodium falciparum* lactate dehydrogenase (*pf*LDH)', *J. Biomol. Struct. Dyn.* **2019**, *37*, 1783–1799. DOI: 10.1080/07391102.2018.1471417.

[2] S. Rout, R. K. Mahapatra, '*Plasmodium falciparum*: Multidrug resistance', *Chem. Biol. Drug Des.* **2019**, *93*, 737–759. DOI: 10.1111/cbdd.13484.

[3] I. A. Adejoro, S. O. Waheed, O. O. Adeboye, 'Molecular docking studies of *Lonchocarpus cyanescens* Triterpenoids as Inhibitors for Malaria', *J. Phys. Chem. B* **2016**, *6*, 1–4. DOI: 10.4172/2161-0398.1000213.

[4] P. Chaniad, M. Mungthin, A. Payaka, P. Viriyavejakul, C. Punsawad, 'Antimalarial properties and molecular docking analysis of compounds from *Dioscorea bulbifera* L. as new antimalarial agent candidates', *BMC Complementary Altern. Med.* **2021**, *21*, 144. https://doi.org/10.1186/s12906-021-03317-y.

[5] N. A. Bispo, R. Culleton, L. A. Silva, P. Cravo, 'A systemic *in silico* search for target similarity identifies several approved drugs with potential activity against the *Plasmodium falciparum* apicoplast', *PLoS One* **2013**, *8*, 59288. DOI: 10.1371/journal.pone.0059288.

[6] J. Vennerstrom, E. Nuzum, R. Miller, A. Dorn, L. Gerena, '8-Aminoquinolines Active against Blood Stage *Plasmodium falciparum in Vitro* Inhibit Hematin Polymerization', *Antimicrob. Agents Chemother.* **1999**, *43*, 598–602. https://www.ncbi.nlm.nih.gov/pmc/articles/PMC89166/.

[7] V. F. Waingeh, A. T. Groves, J. A. Eberle, 'Binding of Quinoline-Based Inhibitors to *Plasmodium falciparum* Lactate Dehydrogenase: A Molecular Docking Study', *Open J. Biophys.* **2013**, *3*, 285–290. https://doi.org/10.4236/ojbiphy.2013.34034.

[8] S. Kumar, T. R. Bhardwaj, D. N. Prasad, R. K. Singh, 'Drug targets for resistant malaria: Historic to future perspectives', *Biomed. Pharmacother.* **2018**, *104*, 8–27.

 © 2022 The Authors. Chemistry & Biodiversity Published by Wiley-VHCA AG

[9] Z. O. Ibraheem, R. Abd Majid, S. M. Noor, H. M. Sedik, R. Basir, 'Role of Different *Pf*crt and *Pf*mdr-1 Mutations in Conferring Resistance to Antimalaria Drugs in *Plasmodium falciparum*', *Malar. Res. Treat.* **2014**, *2014*, 1–17. https://doi.org/10.1155/2014/950424.

[10] M. A. Pfaller, D. J. Krogstad, A. R. Parquette, P. N. Dinh, '*Plasmodium falciparum*: stage-specific lactate production in synchronised cultures', *Exp. Parasitol.* **1982**, *54*, 391–396. DOI: 10.1016/0014-4894(82)90048-0.

[11] D. L. Vander Jagt, L. A. Hunsaker, N. M. Campos, B. R. Baack, 'D-lactate production in erythrocytes infected with *Plasmodium falciparum*' *Mol. Biochem. Parasitol.* **1990**, *42*, 277–284. DOI: 10.1016/0166-6851(90)90171-H.

[12] E. F. Roth Jr., M. C. Calvin, I. Max-Audit, J. Rosa, R. Rosa, 'The enzymes of the glycolytic pathway in erythrocytes infected with *Plasmodium falciparum* malaria parasites' *Blood* **1988**, *72*, 1922–1925. https://doi.org/10.1182/blood.V72.6.1922.1922.

[13] W. M. Brown, C. A. Yowell, A. Hoard, T. A. Vander Jagt, L. A. Hunsaker, L. M. Deck, D. L. Vander Jagt, 'Comparative structural analysis and kinetic properties of lactate dehydrogenases from the four species of human malarial parasites', *Biochemistry* **2004**, *43*, 6219–6229. DOI: 10.1021/bi049892w.

[14] C. R. Dunn, M. J. Banfield, J. J. Barker, C. W. Higham, K. M. Moreton, D. Turgut-Balik, R. L. Brady, J. J. Holbrook, 'The structure of lactate dehydrogenase from *Plasmodium falciparum* reveals a new target for antimalarial design', *Nat. Struct. Biol.* **1996**, *3*, 910–915. DOI; 10.1038/nsb1196–910.

[15] A. Alam, M. Neyaz, S. I. Hasan, 'Exploiting unique structural and functional properties of malarial glycolytic enzymes for antimalarial drug development', *Malar. Res. Treat.* **2014**, *2014*, 1–13. DOI: 10.1155/2014/451065.

[16] S. McClendon, N. Zhadin, R. Callender, 'The Approach to the Michaelis Complex in Lactate Dehydrogenase: The Substrate Binding Pathway', *Biophys. J.* **2005**, *89*, 2024–2032. DOI: 10.1529/biophysj.105.062604.

[17] D. M. Shadrack, S. S. Nyandoro, J. J. E. Munissi, E. B. Mubofu, 'In silico evaluation of antimalarial agents from *Hoslundia opposite* as inhibitors of *plasmodium falciparum* lactate dehydrogenase (*pf*LDH) enzyme', *Comput. Mol. Biosc.* **2016**, *6*, 23–32. https://doi.org/10.4236/cmb.2016.62002.

[18] J. R. E. T. Pineda, R. Callender, S. D. Schwartz, 'Ligand Binding and Protein Dynamics in Lactate Dehydrogenase', *Biophys. J.* **2007**, *93*, 1474–1483. DOI: 10.1529/biophysj.107.106146.

[19] P. Tang, J. Xu, C. L. Oliveira, Z. J. Li, S. Liu, 'A mechanistic kinetic description of lactate dehydrogenase elucidating cancer diagnosis and inhibitor evaluation', *J. Enzyme Inhib. Med. Chem.* **2017**, *32*, 564–571. doi: 10.1080/14756366.2016.1275606.

[20] L. Qiu, M. Gulotta, R. Callender, 'Lactate Dehydrogenase Undergoes a Substantial Structural Change to Bind its Substrate', *Biophys. J.* **2007**, *93*, 1677–1686. doi: 10.1529/biophysj.107.109397.

[21] W. M. Oluyemi, B. B. Samuel, H. Kaehlig, M. Zehl, S. Parapini, S. D'Alessandro, D. Taramelli, L. Krenn, 'Antiplasmodial activity of triterpenes isolated from the methanolic leaf extract of *Combretum racemosum* P. Beauv.', *J. Ethnopharmacol.* **2020**, *247*, 1–7. DOI: 10.1016/j.jep.2019.112203.

[22] J. A. Read, K. W. Wilkinson, R. Tranter, R. B. Sessions, R. L. Brady, 'Chloroquine Binds in the Cofactor Binding Site of Plasmodium falciparum Lactate Dehydrogenase', *J. Biol. Chem.* **1999**, *274*, 10213–10218. doi: 10.1074/jbc.274.15.10213.

[23] M. S. Shapovalov, R. L. Dunbrack Jr., 'A Smoothed Backbone-Dependent Rotamer Library for Proteins Derived from Adaptive Kernel Density Estimates and Regressions', *Structure* **2011**, *19*, 844–858.

[24] J. Wang, W. Wang, P. A. Kollman, D. A. Case, 'Automatic atom type and bond type perception in molecular mechanical calculations', *J. Mol. Graphics Modell.* **2006**, *25*, 247–260.

[25] O. Trott, A. J. Olson, 'AutoDock Vina: Improving the speed and accuracy of docking with a new scoring function, efficient optimisation and multithreading', *J. Comput. Chem.* **2010**, *31*, 455–461. DOI: 10.1002/jcc.21334.

[26] J. O. Olanlokun, A. F. OLotu, O. M. David, T. O. Idowu, E. M. Soliman, O. O. Olorunsogo, 'A novel compound purified from *Alstonia boonei* inhibits *Plasmodium falciparum* Lactate dehydrogenase and Plasmepsin II', *J. Biomol. Struct. Dyn.* **2019**, *37*, 2193–2200. DOI: 10.1080/07391102.2018.1483840.

[27] A. T. Adewumi, M. B. Ajadi, O. S. Soremekun, M. E. S. Soliman, 'Thompson loop: Opportunities for antitubercular demethylmenaquinone methyltransferase protein', *RSC Adv.* **2020**, *10*, 23466–23483. https://doi.org/10.1039/D0RA03206A.

[28] P. Ramharack, M. E. S. Soliman, 'Zika virus NS5 protein potential inhibitors: an enhanced *in silico* approach in drug discovery', *J. Biomol. Struct. Dyn.* **2018**, *36*, 1118–1133. doi: 10.1080/07391102.2017.1313175.

[29] J. P. Ryckaert, G. Ciccotti, H. J. C. Berendsen, 'Numerical integration of the Cartesian equations of motion of a system with constraints: Molecular dynamics of n-alkanes', *J. Comput. Phys.* **1977**, *23*, 327–341. https://doi.org/10.1016/0021-9991(77)90098-5.

[30] A. T. Adewumi, A. Elrashedy, O. S. Soremekun, M. B. Ajadi, M. E. S. Soliman, 'Weak spots inhibition in the *Mycobacterium tuberculosis* antigen 85 C target for antitubercular drug design through selective irreversible covalent inhibitor-SER124', *J. Biomol. Struct. Dyn.* **2020**. DOI: 10.1080/07391102.2020.1844061.

[31] W. Humphrey, A. Dalke, K. Schulten, 'VMD: Visual Molecular Dynamics William', *J. Mol. Graphics* **1996**, *14*, 33–38. DOI: 10.1016/j.carbon.2017.07.012.

[32] U. Kalathiya, M. Padariya, M. Baginski, 'Structural, functional, and stability change predictions in human telomerase upon specific point mutations', *Sci. Rep.* **2019**, *9*,1–13. https://www.nature.com/articles/s41598-019-45206-y.

[33] E. Seifert, 'OriginPro 9.1: Scientific data analysis and graphing software-software review', *J. Chem. Inf. Model.* **2014**, *54*, 1552–1552. https://doi.org/10.1021/ci500161d.

[34] V. Gapsys, S. Michielssens, J. H. Peters, B. L. de Groot, H. Leonov, 'Calculation of Binding Free Energies', *Methods Mol. Biol.* **2015**, *1215*, 173–209, DOI: 10.1007/978-1-49391465-4.

[35] S. Genheden, U. Ryde, 'The MM/PBSA and MM/GBSA methods to estimate ligand-binding affinities', *Expert Opin. Drug Discovery* **2015**, *10*, 449–461. https://doi.org/10.1517/17460441.2015.1032936.

 © 2022 The Authors. Chemistry & Biodiversity Published by Wiley-VHCA AG

[36] I. Bjij, S. Khan, R. Betz, D. Cherqaoui, M. E. S. Soliman, 'Exploring the structural mechanism of covalently bound E3 ubiquitin ligase: Catalytic or allosteric inhibition?', *Protein J.* **2018**, *37*, 500–509. https://doi.org/10.1007/s10930-018-9795-5.

[37] M. Y. Lobanov, N. S. Bogatyreva, O. V. Galzitskaya, 'Radius of gyration as an indicator of protein structure compactness', *Mol. Biol.* **2008**, *42*, 623–628. DOI: 10.1134/S0026893308040195.

[38] O. D. Lopina, 'Enzyme inhibitors and activators', Intech open science, chapter 11, section 3.2 **2017**. https://doi.org/10.5772/67248.

[39] F. A. Olotu, M. E. S. Soliman, 'From mutational inactivation to aberrant gain-of-function: unraveling the structural basis of mutant p53 oncogenic transition', *J. Cell. Biochem.* **2018**, *119*, 2646–52. DOI: 10.1002/jcb.26430.

[40] F. B. Akher, A. Farrokhzadeh, F. A. Olotu, C. Agoni, M. E. S. Soliman, 'The irony of chirality – unveiling the distinct mechanistic binding and activities of 1-(3-(4amino-5-(7-methoxy-5-methylbenzo[b]thiophen2-yl)-7H-pyrrolo[2,3-d]pyrimidin-7-yl)pyrrolidin1-yl)prop-2-en-1-one enantiomers as irreversible covalent FGFR4 inhibitors', *Org. Biomol. Chem.* **2019**, *17*, 1176–1190. DOI: 10.1039/c8ob02811g.

[41] U. Ndagi, N. N. Mhlongo, M. E. Soliman, 'The impact of Thr91 mutation on c-Src resistance to UM-164: Molecular dynamics study revealed a new opportunity for drug design', *Mol. BioSyst.* **2017**, *13*, 1157–1171. https://doi.org/10.1039/c6mb00848h.

[42] I. A. Emmanuel, F. Olotu, C. Agoni, M. E. S. Soliman, 'Broadening the horizon: Integrative pharmacophore-based and cheminformatics screening of novel chemical modulators of mitochondria ATP synthase towards interventive Alzheimer's disease therapy', *Med. Hypotheses* **2019**, *130*, 109277. https://doi.org/10.1016/j.mehy.2019.109277.

[43] J. W. Pitera, 'Expected distributions of root-mean-square positional deviations in proteins', *J. Phys. Chem. B* **2014**, *118*, 6526–30. DOI: 10.1021/jp412776d.

[44] A. Bornot, C. Etchebest, A. G. De Brevern, 'Predicting protein flexibility through the prediction of local structures', *Proteins Struct. Funct. Bioinf.* **2011**, *79*, 839–52. DOI: 10.1002/prot.22922.

[45] V. Z. Spassov, L. Yan, P. K. Flook, 'The dominant role of side-chain backbone interactions in structural realisation of amino acid code. ChiRotor: a side-chain prediction algorithm based on side-chain backbone interactions', *Protein Sci.* **2007**, *16*, 494–506. doi: 10.1110/ps.062447107.

[46] H. Tanwar, C. G. P. Doss, 'An integrated computational framework to assess the mutational landscape of a-L-idurondase IDUA gene', *J. Cell. Biochem.* **2018**, *119*, 555–565. https://doi.org/10.1002/jcb.26214.

[47] E. Papaleo, G. Saladino, F. L. Gervasio, M. Lambrughi, R. Nussinov, 'The Role of Protein Loops and Linkers in Conformational Dynamics and Allostery', *Chem. Rev.* **2016**, *116*, 6391–6423. DOI: 10.1021/acs.chemrev.5b00623.

Received August 11, 2021
Accepted November 29, 2021

 © 2022 The Authors. Chemistry & Biodiversity Published by Wiley-VHCA AG